Electronic Supplementary Material (ESI) for Materials Horizons.

Fabrication of Textile-based Triboelectric Nanogenerator toward high-efficiency energy harvesting and material recognition

Junjun Huang[a,c], Sanlong Wang[a,b], Xingke Zhao[a,c], Wenqing Zhang[a,b], Zhenming Chen[a,c], Rui Liu[a,b], Peng Li[c***], Honglin Li[a,b,c**] and Chengmei Gui[a,b,c*]

[a] *School of Energy Materials and Chemical Engineering, Hefei University, Hefei City, 230601 China*
[b] *School of Chemistry and Chemical Engineering, Chaohu University, Hefei City, 230009, China*
[c] *Guangxi Key Laboratory of Calcium Carbonate Resources Comprehensive Utilization, College of Materials and Chemical Engineering, Hezhou University, Hezhou City, 542899, China*

Corresponding Authors:
***Peng Li E-mail: lipeng163163163@163.com
**Honglin Li E-mail: lihonglin163163@163.com
*Chengmei Gui E-mail: guichengmei@163.com

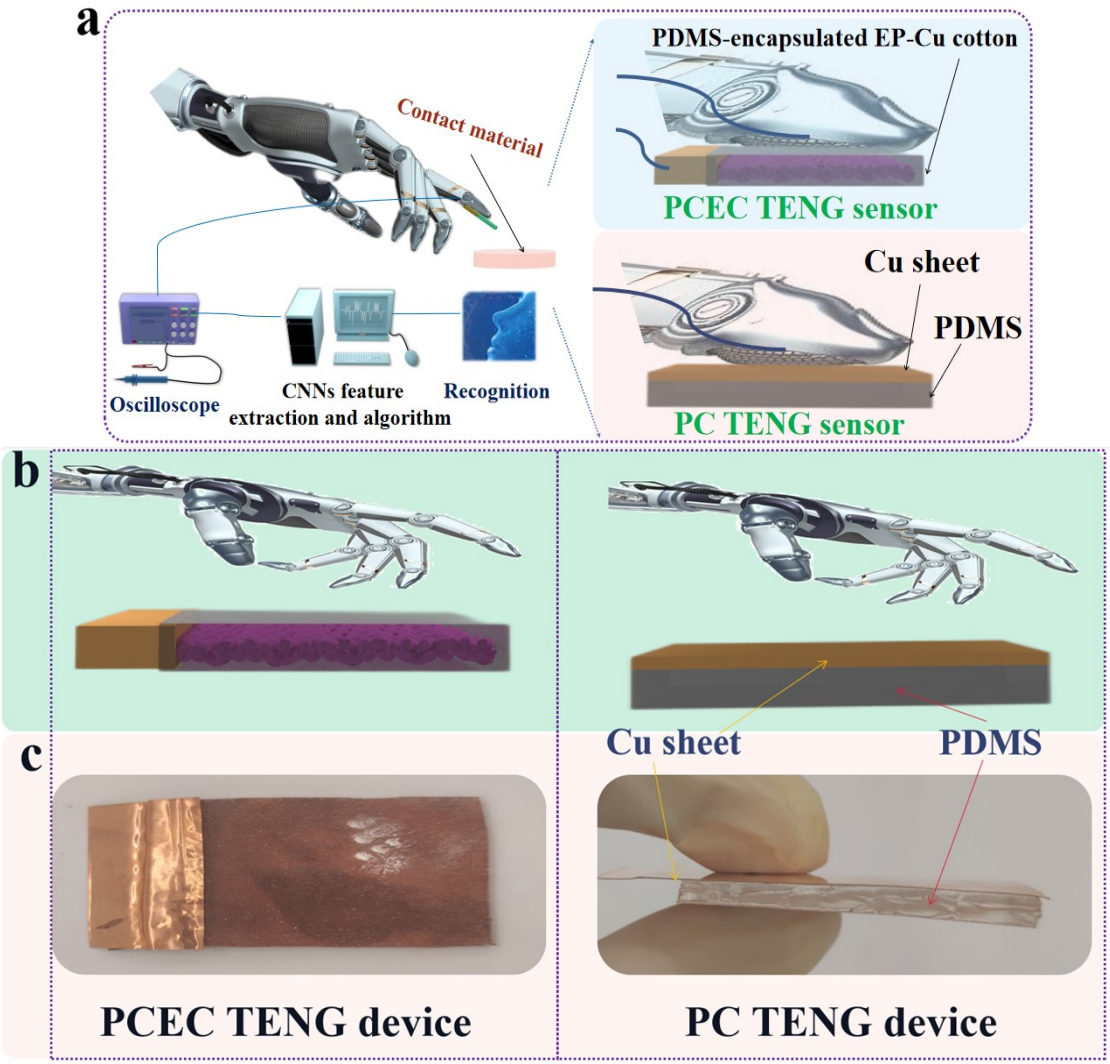

Fig. S1. (a) schematic diagram of the application with intelligent prosthesis. Structural diagram (b) and optical photograph (c) of PC and PCEC TENG devices

the schematic diagram of the application with intelligent prosthesis are displayed in Fig. S1 a. In addition, Figs. S1 b and c displayed structural diagram of PC and PCEC TENG devices. Similar to a closed sandwich structure, the EP-Cu cotton is located in the middle layer, one side leads out the electrode (positive electrode), the others are sealed in the PDMS layer (PCEC device). In this structure, the polymer surface acts as a negative electrode. To further verify the unique characteristics of PCEC TENG device, we fabricated the conventional TENG device of single electrode mode: triboelectric material (PDMS layer) coated on the Cu sheet surface (PC device). the thickness of the two devices is 0.24 cm in this work. Corresponding optical photograph of PC and PCEC TENG devices is displayed in Fig. S1 c.

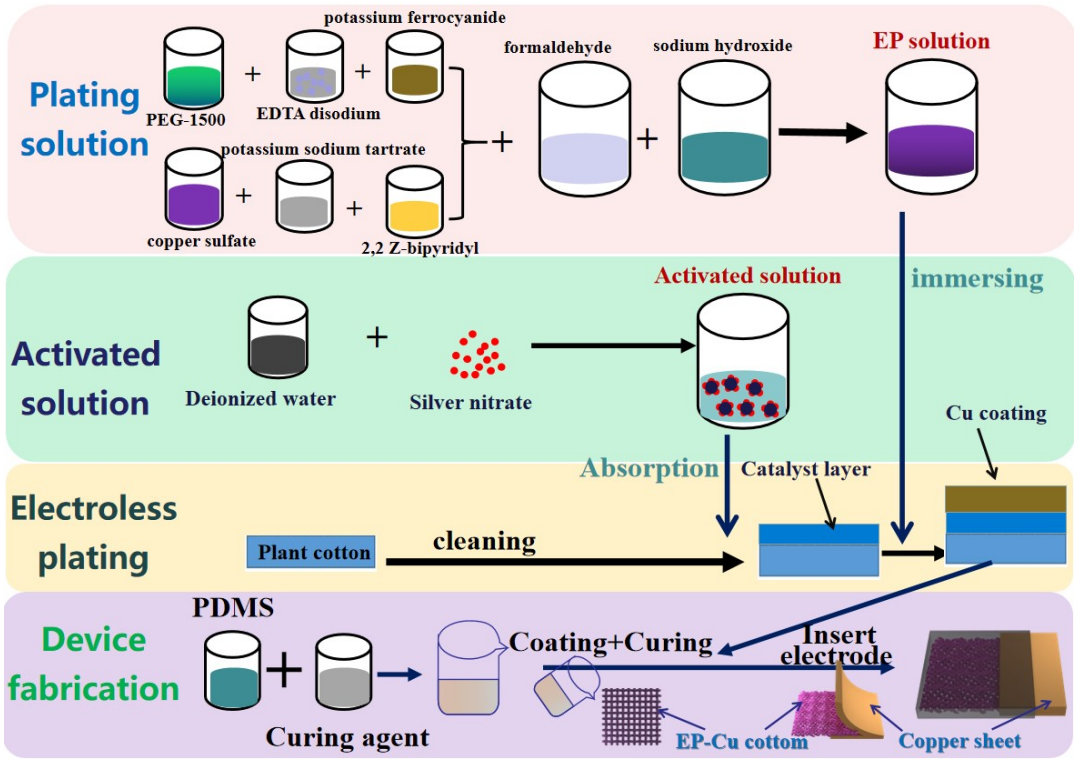

Fig. S2. Schematic diagram of the fabrication process of PCEC TENG device

Fabrication of Catalytic layer: $AgNO_3$ (40 g, 3 g/L) solution was fabricated and use to catalytic solution. The cotton sheet was cleaned by degreased solution, deionized water and acetone beforehand, in sequence at 333 K for 60 min, respectively. The cleaned substrate surface immersing in catalytic solution for 30 min. Afterward, the sample was rinsed in a water bath for several minutes followed by drying with blown nitrogen. As a result, catalytic layer by means of silver nanoparticles/polymer brush structure on sample surface was fabricated (AC-Ag cotton).

Electroless P*lating: The AC-Ag cotton was electrolessly plated using a reported copper electroless plating solution. The components of the plating solution is 2,2 Z-bipyridyl 0.01 g/L; EDTA disodium 15.5 g/L; PEG-1500 0.8 g/L; copper sulfate 15 g/L; sodium hydroxide 10.5 g/L; formaldehyde 11 ml/L; potassium ferrocyanide 0.08 g/L and potassium sodium tartrate 10 g/L. Ingredients and deionized water were first mixed and heated to 40°C. After the bath was allowed to stabilize to the plating

temperature, the catalytic layer-coated cotton was placed in the bath for the desired time. After plating, the plated sample was rinsed in a water bath for several minutes followed by drying and heating with blown nitrogen. The pH was measured using a pH meter, and found to maintain a steady pH of between 11.5 and 12 during the entire plating run. The schematic diagram of EP-Cu cotton can be seen in Figs. 1a and S2.

Fabrication of PCEC TENG device: The curing agent and PDMS prepolymer (weight ratio of 1:12.5) were mixed. Firstly, the processed PDMS was evenly coated on the glass plate. Afterward, the EP-Cu cotton was inserted into the PDMS layer until it is entirely soaked. We adopt the polymer-encapsulated metal material with higher interfacial contact area to fabricate the PCEC TENG device (Figs. 2a and b iv). Similar to a closed sandwich structure, the EP-Cu cotton is located in the middle layer, as displayed in Figs.2 b i-iv and S2. One side leads out the electrode (positive electrode), the others are sealed in the PDMS layer (PCEC device). In this structure, the polymer surface acts as a negative electrode. After being cured then heated at 120 ^{o}C for 1.5 h. After that, PCEC TENG device was prepared.

Material and Characterization: The cotton composed of 80% cotton and 20% polyester was bought from the Wanchang Weaving Co. Ltd (Jinzhou, China), the gram weight is 105 g/m^2. The other experiments' materials were purchased from Aladdin Chemical Reagent Company (China) and used without further purification. Surface morphology was observed by scanning electron microscopy (SEM, JEOL, JSM-5600LV). Chemical structure was measured by X-ray diffraction (XRD, Rigaku D/max-2550V) and X-ray photoelectron spectroscopy (XPS, Shimazu, AXIS ULTRADLD). XPS spectra was calibrated by using the C1s peak (284.5 eV).

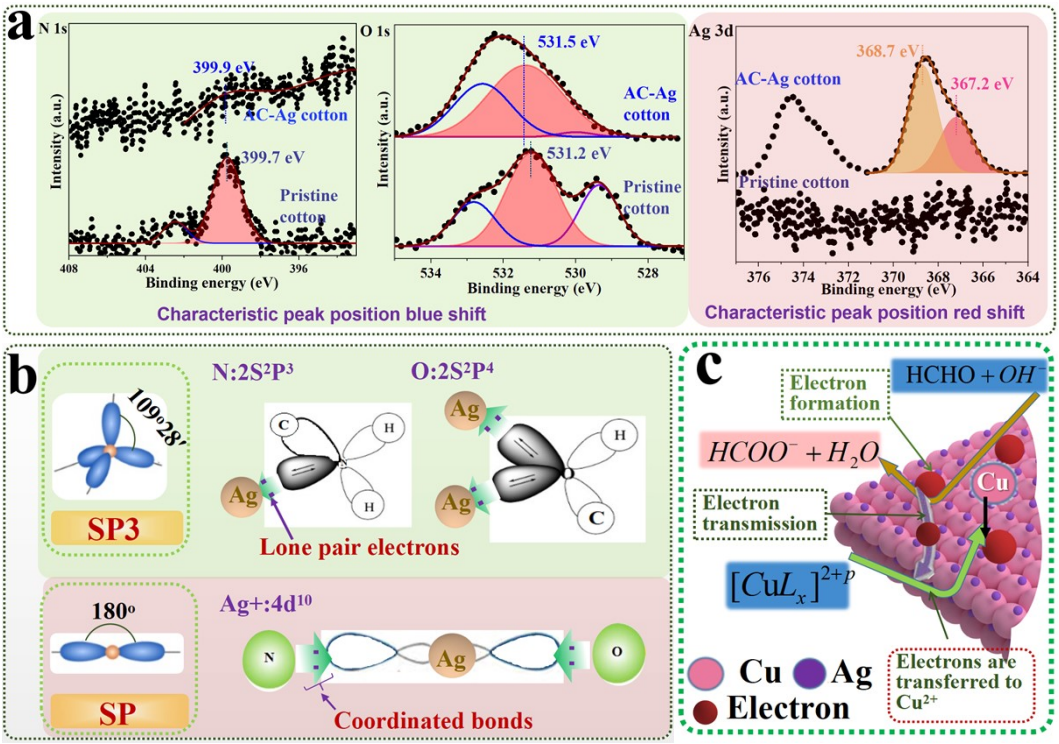

Fig. S3. Mechanism illustration of EP-Cu on cotton. (a) N 1s, O 1s and Ag 3d XPS spectra. (b) schematic illustration of the chemical bonding between the N/O and Ag. (c) Summarized structure of orbital interaction in HCHO on Ag surface

To gain a better understanding of bonding mechanism of substrate/catalytic site interface, XPS was used to analyse the O, N and Ag electronic structure, as displayed in Figures 1e and S3 a. N 1s and O 1s peaks positions in XPS spectrum of AC-Ag cotton were enhanced to 399.9 eV and 531.5eV, respectively, as a result of the more electron being transferred from N and O to Ag nuclei. As anticipated, a new characteristic peak of 367.2 eV is appeared in Ag 3d XPS spectrum of AC-Ag cotton. According to the hybrid orbital theory [42-45], two unoccupied orbitals of Ag *SP* orbital are filled by the lone pair electrons form the O and N *SP3* hybrid orbitals (as displayed in Figure S3 b), which would facilitate the establishment of a strong internal bonding. Ag^{+}/active group ligand as the precursor of nano-particle catalyst was exposed in the light and then converted to FCC Ag nanoparticles. From the results we have obtained, it is concluded that Ag particle was adsorbed on the fiber surface by coordination bonds (Ag-N and Ag-O), as displayed in Figure 1h. Ag particles were evenly distributed on the substrate surface (Figures 1c, e, h and S3 c).

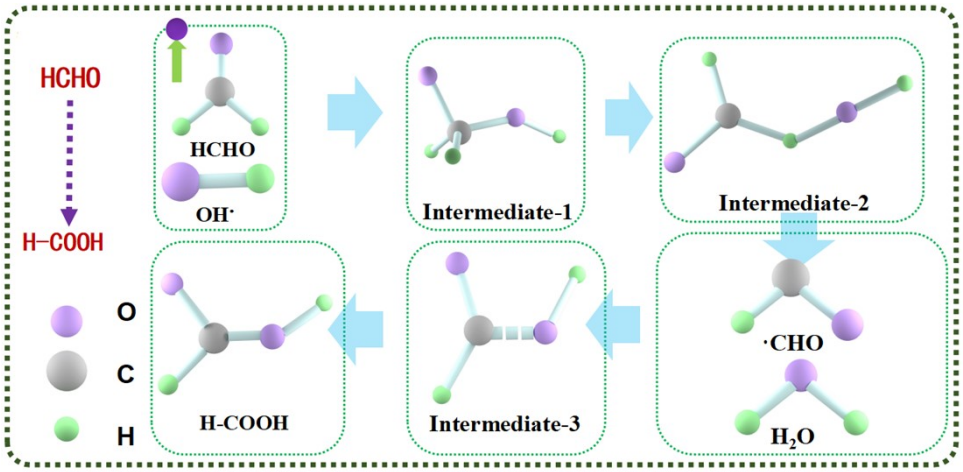

Fig. S4. Summarized structure of orbital interaction in HCHO on Ag surface

According to the traditional understanding of the structure of Ag particles, as shown in Fig. S4, the coupling of HCHO and Ag d-orbitals in EP solution results in the tendency of HCHO moleculesto cling to the catalyst's surface. The metal atom's antibonding orbital is shifted to a lower energy level in the direction of the adsorbent, where there are more electrons. This brings the O particle (·OH in the solution) and C (HCHO) closer together to form C-O bond, this change in structure leads to the formation of intermediate-1. It is important to note that this component creates a free electron. As the reaction proceeds, the C-O deforms when the O and H atoms are in contact, culminating in the creation of intermediate-2. After that, ·CHO and H_2O are formed in the solution. A high-activity ·CHO group that is more likely than not to form a covalent connection with ·OH, result in the formation of H-COOH [1-4]. As a result, under the catalysis of the Ag particle, HCHO was converted into H-COOH. The charge was then transferred to Cu^{2+} via unoccupied Ag d-orbitals, which caused Cu^{2+} to be reduced to Cu atoms. As a result, Cu coating is deposited on cotton surface. As expected, obvious Cu signal is detected in the Figs.1d and e.

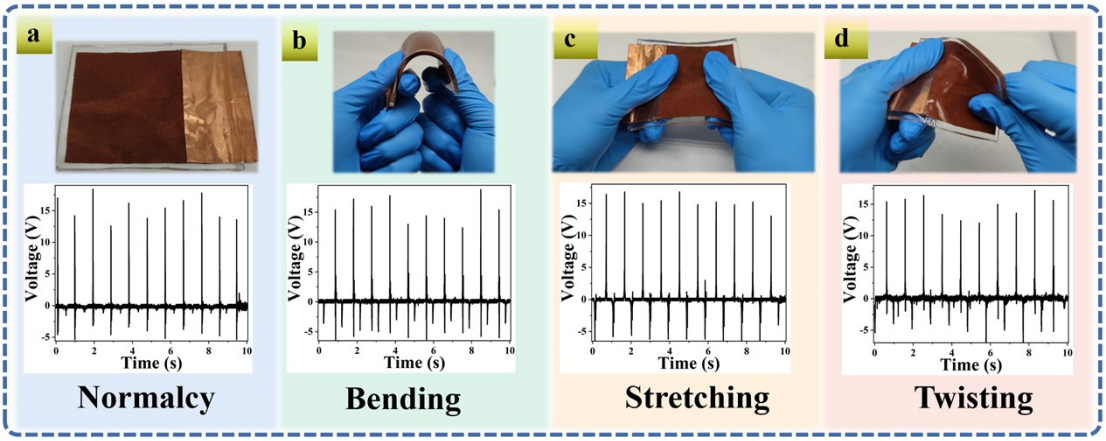

Fig. S5. Stability test of TENG device. Output voltage signal and testing photograph of (a) TENG device and the one after 1000 times (b) bending, (c) stretching and (d) twisting test

It is worth mentioning that high flexibility of the TENG device can maximally ensure the uniform performance for energy harvesting and monitoring. To address this concern, polymer-encapsulated EP-Cu cotton with higher interfacial contact area to fabricate the TENG device (Figs. 1f i-v and S5 a-d) in this work. Similar to a closed sandwich structure, the EP-Cu cotton is located in the middle layer, one side applied for making electrode and lead. Hydrophobic and flexible PDMS shell layer protects the inner EP-Cu cotton and the interface from external damage. As a result, the as-fabricated TENG device has excellent flexibility that can accommodate various motions such as bending, stretching, and twisting (Figs. 1f iv, v and S5 a-d). As displayed in Figs. S5 a-d, the output voltage of TENG before stability test is about 15 V (Figs. S5 a). Its output voltage are also about 15 V after 1000 times (Figs. S5 b) bending, (Figs. S5 c) stretching and (Figs. S5 d) twisting test, indicating the TENG exhibited excellent flexibility.

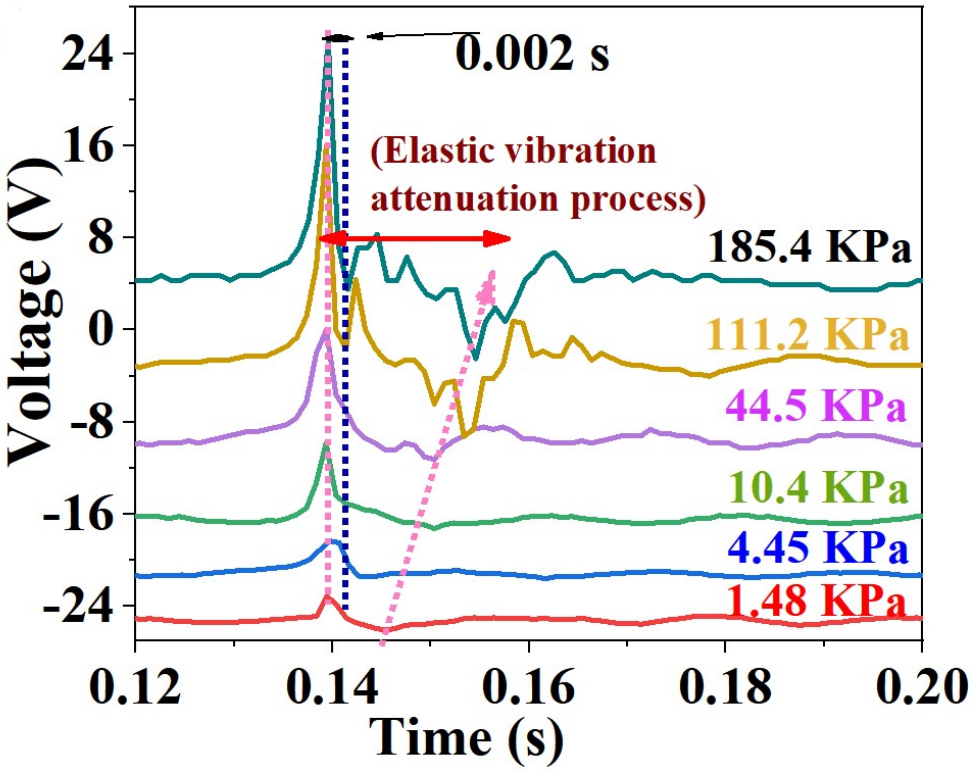

Fig. S6. Output performance of the PCEC TENG device under different external stresses

Meanwhile, the time interval between releasing output and compressing output is about 0.002 s (Fig. S6), indicating it has high sensitivity, laying the foundation for a further application in self-powered sensor. Furthermore, the signal gradually diminished until it disappeared, accordingly, elastic vibration occurred under the action of a force in PDMS layer, the duration of elastic vibration increases gradually with the enhancement of stress. It is worth noting that the shape of the curves is quite different and easy to distinguish, which also indicates that the device working mechanism is difference under different stresses.

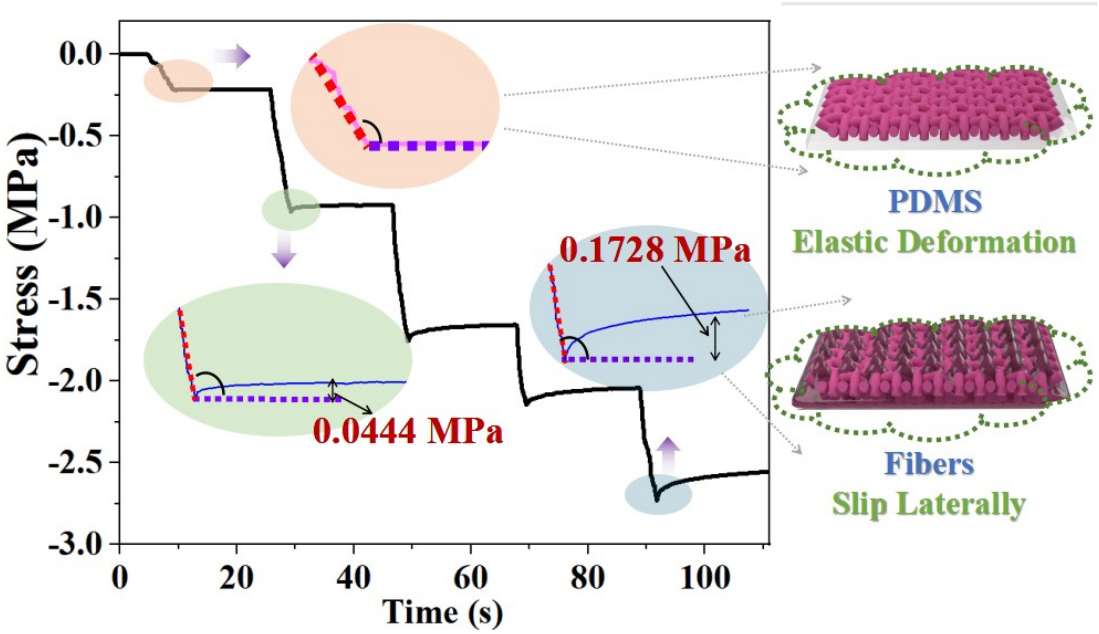

Fig. S7. The relationship between different stress and time on the surface of PCEC TENG device

In order to study the deformation mechanism of samples under different compressive stresses. The different external stresses (0.21 MPa, 0.96 MPa, 1.75 MPa, 2.15 MPa and 2.73 MPa) were applied to the PCEC TENG device surface for about 19 s. The relationship between time and stress on the surface of PCEC TENG device (true stress) was analyzed (Figure S7). To be precise, the creep behavior of sample under different stresses was analyzed. It can be seen that, time has no effect on the true stress when external stresses is 0.21 MPa (without creep behavior), indicating only PDMS compressive strain is established in the PCEC material at lower external stress. Moreover, the true stress decreases gradually to 0.92 MPa with the increase of time, when external stresses is enhanced to 0.96 MPa (creep behavior). Of note, the creep behavior becomes more and more obvious with the increase of external stress, indicating the fibers begin to slip laterally with the formation of larger material strain.

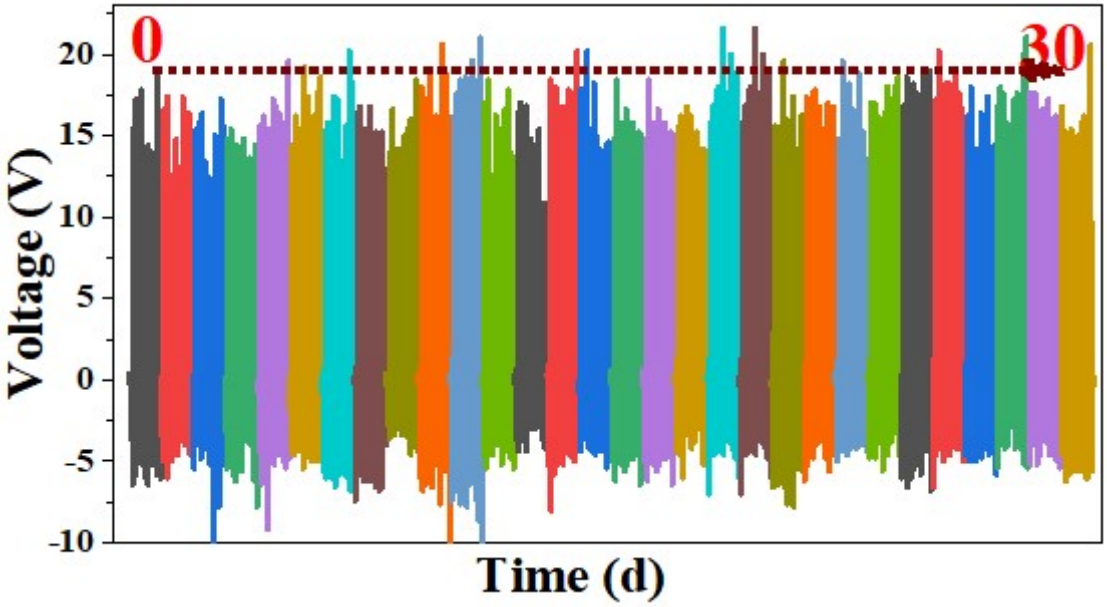

Fig. S8. Stability test of TENG device

It is important to highlight that stability of performance is most important characteristic for practical application of TENG device. We found the device output performance do not even exhibit any obvious fluctuation and measurable degradation with negligible changes, or even a month later (Figure S8), indicating the as-fabricated PCEC device has excellent stability and durability. The reason for this is because hydrophobic and flexible PDMS shell layer protects the inner EP-Cu cotton and the interface from external damage.

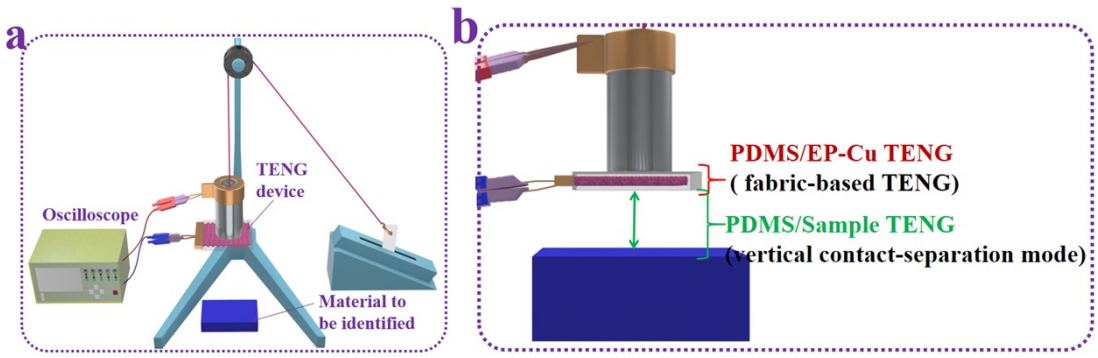

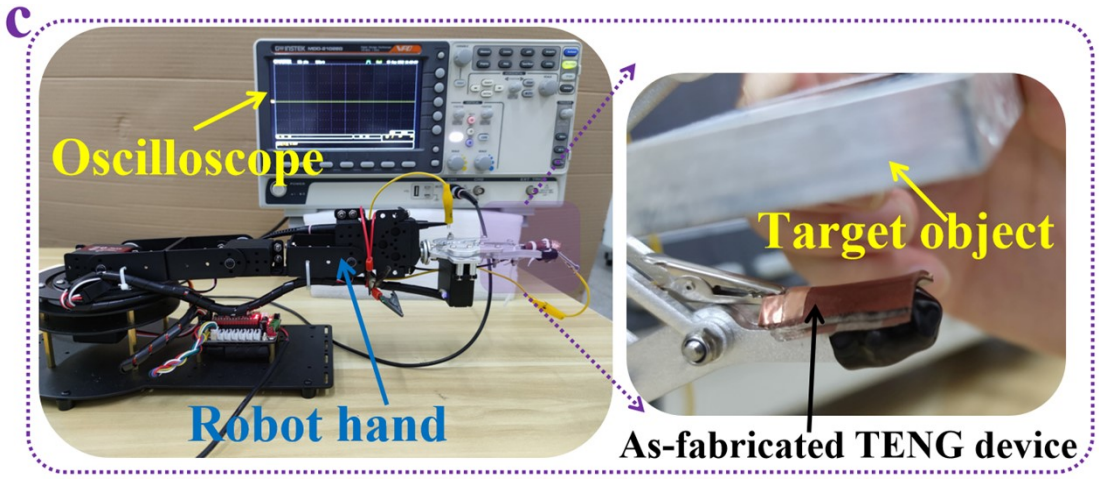

Fig. S9. Schematic diagram for data acquisition. (a,b) Mechanism illustration of data processing and identification and (c) images of experimental setup using the TENG to accurate recognition

Output voltage signals are often influenced by a combination of the contact material, contact pressure, and contact environmental conditions. In this work, the height of the object in free fall remained the same (0.04 m), the mass of weights are 0.75 kg, respectively. The calculated compressive stresses on the devices is 79.5 KPa by formula (1-4). The fixed positions of the device and target material are shown in the Figure S9 a. To be precise, two TENG device, PDMS/EP-Cu (PCEC TENG) and PDMS/sample (Figure S9 b), were established, result in the formation of two sensing signals from the PCEC TENG sensor as it contacts different materials. We concluded that various materials will provide different electrical signals, accompanied by unique characteristics, hence, the triboelectric signals generated by the as-fabricated TENG are capable of sensitive detection for contact materials. The overview and ideal experimental images of the involved intelligent tactile sensing system based on triboelectric signal and deep learning are shown in Figure S9 c, the sensor is fixed on the inside of the manipulator. Extracting characteristics from multiple electrical signals offers exciting opportunities to achieve improving recognition accuracy. With the help of machine learning, more deep-rooted features of the identified materials are captured, and eventually achieve accurate identification independent of the environment.

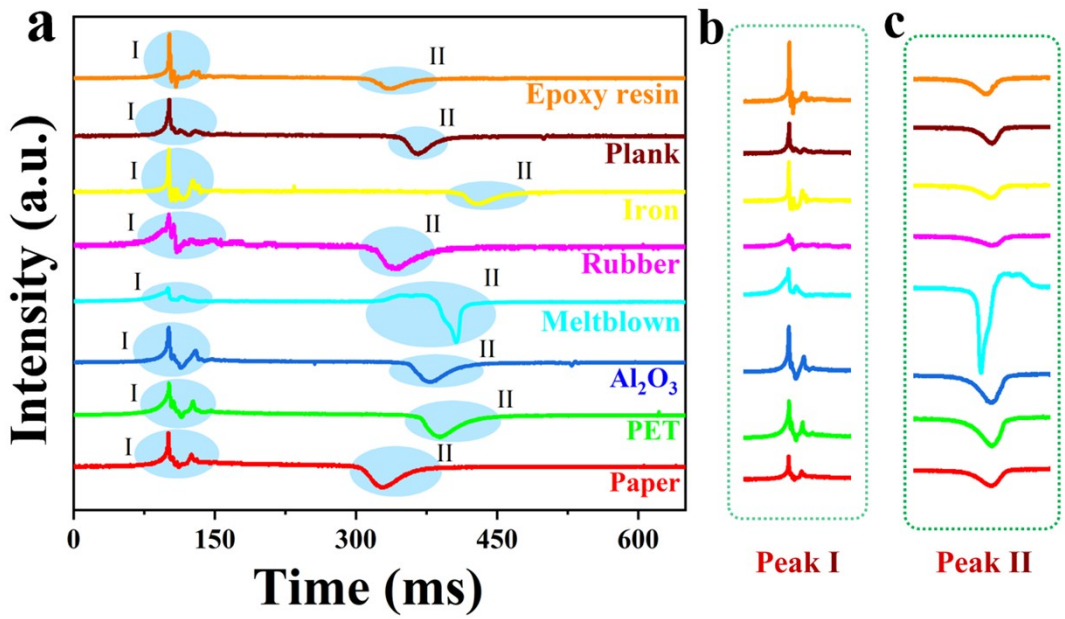

Fig. S10. The sensing signals from the sensor as it contacts different materials (a) and corresponding partial enlarged diagram (c,d)

The characteristics (peak position, spacing and shape) of signal curve from the TENG-based tactile sensor as the TENG impact the material surface are used to recognize the unknown and contact material. The signals are presented in Fig. S10 a, obviously, the shape, number of characteristic peaks and distance between two peaks are different, i.e., the relative intensities of contact/separation peaks were inconsistent, the distance between the two peaks on the curve is also different.

More importantly, the signal from the PCEC TENG device as it contacts different materials is a combination of output signals from PDMS/EP-Cu (Peak I in Fig. S10 b) and PDMS/recognize object (Peak II in Fig. S10 b) device. To be exact, there are two TENG devices (PDMS/EP-Cu and PDMS/recognize object) that work when the as-fabricate PCEC TENG devices under 12.4-139 KPa stress.

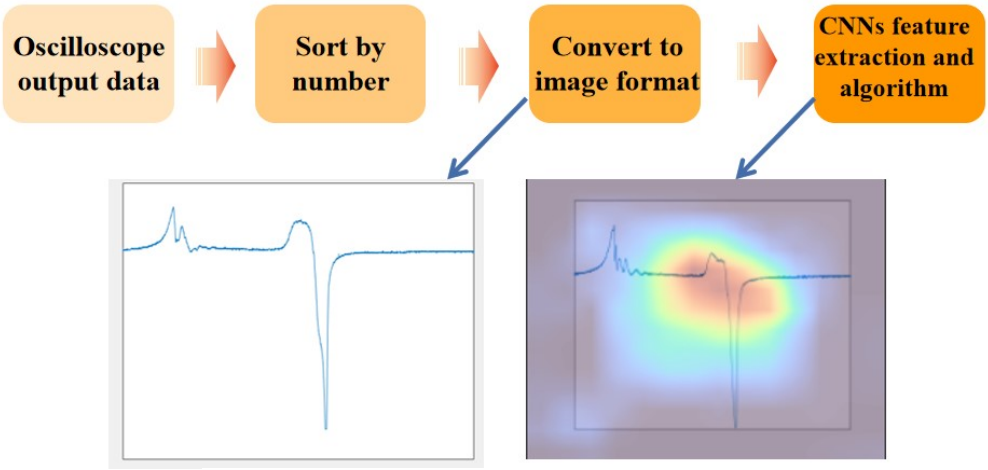

Fig. S11. Workflow of as-fabricate TENG touch sensing

Figure S11 displayed workflow of as-fabricate TENG touch sensing. The data from oscilloscope is numbered, formatted (convert to image format), CNNs feature extracted and recognized sequentially, then we can get the recognition result.

REFERENCES

[1] X. Wang, S.I. Choi, L.T. Roling, et al., Palladium-platinum core-shell icosahedra with substantially enhanced activity and durability towards oxygen reduction. Nat. Commun. 2015, 7594, 7594, https://doi.org/10.1038/ncomms8594.

[2] M. Kunimoto, T. Shimada, S. Odagiri, et al., Density functional theory analysis of reaction mechanism of hypophosphite ions on metal surfaces. J Electrochem. Soc. 2011, 158, 585-589. https://doi.org/10.1149/1.3609000.

[3] M. Kunimoto, H. Nakai, T. Homma, Density functional theory analysis for orbital interaction between hypophosphite ions and metal surfaces. J Electrochem. Soc. 2011, 158, 626-633. https://doi.org/10.1149/1.3623782.

[4] J.J. Cai, M.H. Zhou, Y.W. Pan, et al., Extremely efficient electrochemical degradation of organic pollutants with co-generation of hydroxyl and sulfate radicals on blue-TiO_2 nanotubes anode. Appl. Catal. B-Environ 2019, 257, 117902. https://doi.org/10.1016/j.apcatb.2019.117902.

[5] Y. Xi, J. Wang, Y. Zi, et al., High efcient harvesting of underwater ultrasonic wave energy by triboelectric nanogenerator. Nano Energy 2017, 38, 101-108. https://doi.org/10.1016/j.nanoen.2017.04.053.

[6] X. Wei, Z. Zhao, C. Zhang, et al., All-weather droplet-based triboelectric nanogenerator for wave energy harvesting. ACS Nano 2021, 15, 13200-13208. https://doi.org/10.1021/acsnano.1c02790.

[7] H.J. Kim, E.C. Yim, J.H. Kim, et al., Bacterial nano-cellulose triboelectric nanogenerator. Nano Energy 2017, 33, 130-137. https://doi.org/10.1016/j.nanoen.2017.01.035.

[8] M. Salari, M.S. Khiabani, R.R. Mokarram, et al., Preparation and characterization of cellulose nanocrystals from bacterial cellulose produced in sugar beet molasses and cheese whey media. Int. J Biol. Macromol. 2019, 122, 280-288. https://doi.org/10.1016/j.ijbiomac.2018.10.136.